Artificial Organs
28(11):1002–1015, Blackwell Publishing, Inc.

A Tensor-based Measure for Estimating Blood Damage

*†Dhruv Arora, *‡Marek Behr, and †§Matteo Pasquali

**Department of Mechanical Engineering and Materials Science; †Computer and Information Technology Institute (CITI), Rice University, Houston, TX, U.S.A.; ‡Lehrstuhl für Numerische Mechanik, Technische Universität München, Garching, Germany; and §Department of Chemical Engineering, Rice University, Houston, TX, U.S.A.*

Abstract: Implantable ventricular assist devices give hope of a permanent clinical solution to heart failure. These devices, both pulsatile- and continuous-flow, are presently used as medium-term bridge to heart transplant or recovery. While long-term use of continuous-flow axial and centrifugal pumps is being explored, the excessive level of blood damage in these devices has emerged as a design challenge. Blood damage depends both on shear stress and exposure time, and device designers have relied traditionally on global space- and time-averaged estimates from experimental studies to make design decisions. Measuring distributions of shear stress levels and the blood cell's exposure to these conditions in complex rotary pump flow is difficult. On the other hand, computational fluid dynamics (CFD) is now being used as a tool for designing viable devices, offering more detailed information about the flow field. A tensor-based blood damage model for CFD analysis is proposed here. The model estimates the time- and space-dependent strain experienced by individual blood cells and correlates it to blood damage data from steady shear flow experiments. The blood cells are modeled as deforming droplets and their deformation is tracked along the pathlines of a computed flow. The model predicts that blood cells in a rapidly fluctuating shear flow can sustain high shear stress levels for very short exposure time without deforming considerably. In the context of mechanical modeling of the implantable Gyro blood pump being developed at Baylor College of Medicine, this suggests that blood cells traversing regions of highly fluctuating shear stress rapidly may not hemolyze significantly.
Key Words: Ventricular assist device—Computational fluid dynamics—Red blood cell—Hemolysis—Droplet deformation.

Every year 800 000 new cases of heart disease are reported in the United States; by a conservative estimate, 50 000 patients can use a new heart, but only 2500 donor hearts are available annually (1). Similar statistics prevail worldwide. While a patient waits for a healthy donor heart, life-saving medical treatment with a ventricular assist device (VAD) is currently the only hope for the ailing heart. Since the first successful VAD implant in 1966 by DeBakey (1), VAD technology has progressed to a point where these devices are being used as a medium-term bridge to transplant. Presently, the development of the third generation VAD devices with magnetically suspended no-contact bearings is underway (2), and these devices can potentially provide an alternate treatment to heart transplant.

The development of VADs poses a tremendous challenge because the working fluid in these devices is blood, which has a highly complex, flow-dependent physical and chemical nature. Blood is a suspension of formed elements—red blood cells (RBCs), white blood cells, and platelets—in a Newtonian liquid (plasma) of viscosity 1 mPa·s (cP). At normal concentrations, blood behaves as a non-Newtonian fluid. Most traditional blood-handling devices were designed for Newtonian fluids and adapted for blood flow applications after prolonged in vivo animal trials. Besides being time-consuming and laborious, the process was costly, and by necessity, involved only a handful of candidate designs.

There are two aspects of VAD design—hydraulic and hematologic. The hydraulic design ensures that the pump delivers appropriate flow rates against a given pressure head; the hematologic design aims at minimizing the blood damage in the pump. Hydraulic design methods for centrifugal pumps are well devel-

Received October 2003; revised April 2004.
Address correspondence and reprint requests to Dr. Marek Behr, Lehrstuhl für Numerische Mechanik, Technische Universität München, D-85747 Garching, Germany. E-mail: behr@lnm.mw.tum.de or Dr. Matteo Pasquali, Department of Chemical Engineering, MS 362, PO Box 1892, Houston, TX 77251-1892, U.S.A. E-mail: mp@rice.edu

oped, and the conservation equations governing the flow are known completely (3–9). Thus, the hydraulic design process of the VAD is well-formulated. Recently, computational fluid dynamics (CFD) has emerged as a reliable hydraulic design tool for VADs. Since a 3-dimensional non-Newtonian CFD simulation of a blood pump is a formidable task, several groups have conducted Newtonian CFD analysis of both pulsatile- and continuous-flow blood pumps over the past decade (5–9) and reported hydraulic parameters such as flow rate, pressure head, shear stress, velocity profiles, location and size of stagnation zones, and local shear rate. These parameters provide crucial quantitative information for hydraulic design, and qualitative information for hematologic design. Burgreen et al. reviewed the CFD-based holistic design process of rotary blood pumps and pointed to the need for coupling between hydraulic and hematologic design (10).

Blood damage (hemolysis) and blood aggregation (thrombosis) are two important features of hematologic design (11). How these processes occur in complex flow situations is not yet understood clearly. As a result, unlike the hydraulic design process, the hematologic design problem is not well-formulated. Previous works on hematologic design have relied on test-loop experiments with human or animal blood to obtain actual measurements of hemolysis (12–14). The experimentally measured hemolysis values, while being accurate, provide only global, time- and space-averaged estimates by treating the blood pump as one complete unit. It is not possible to obtain a local estimate of hemolysis in a section of the blood pump in test-loop experiments. Flow visualization techniques have been used to estimate qualitatively local hemolysis characteristics of the pumps (15). Thus, understanding the effect of design changes on device performance (e.g., minimal hemolysis) is a slow, expensive, and laborious process. On the other hand, CFD-based hemolysis prediction is quicker, cheaper, can easily show the effect of localized design modification on pump performance, and can also assess the aggregate effect of multiple design changes. However, in order to succeed, it requires a realistic model of blood damage. While the flow in blood pumps is 3-dimensional and unsteady, blood damage models are available only for simple steady shear flows.

In our previous work on computational analysis of implantable ventricular assist devices (3,4), we reported hydraulic measures; here we propose a model for predicting hemolysis based on instantaneous deformation of RBCs in a general flow. This model accounts for blood cell properties, and is tuned with the experimental data on flow-induced RBC deformation and hemolysis. In this article, we review the literature on hemolysis in the next section. The governing equations describing the blood flow are discussed in the following section. A blood damage model based on RBC deformation can be developed only with a clear understanding of RBC behavior in shear flow, which has been reported in several experimental studies; thus, the next section details the RBC behavior in steady shear flow as observed in viscometric experiments reported in the literature, and discusses a hemolysis-stress-exposure correlation. Then we set out the tensor-based blood cell deformation model; the parameters of this model are then tuned with available experimental data. The instantaneous blood cell deformation is related to hemolysis prediction. Implementational details of hemolysis prediction in homogeneous and inhomogeneous flows are given, followed by numerical experiments, which compare the new hemolysis predictions with the traditional methods. Finally, we conclude with a summary and future directions.

LITERATURE REVIEW: HEMOLYSIS IN BLOOD PUMPS

RBCs are the largest constituent of blood, and hemolysis refers to premature damage of RBCs, which otherwise have a normal life span of 120 days in a healthy person (16). While the body can adapt to a moderately abnormal depletion rate of RBC, excessive hemolysis may lead to a low RBC count and a state of hemolytic anemia. Apart from low RBC count response, the plasma free hemoglobin is toxic for the kidneys (2), and can eventually lead to multiple organ failure. Hemolysis can happen due to various pathological conditions or external factors, which can all be reduced to four basic mechanisms: colloid osmotic lysis, perforation of a cell, excessive deformation or fragmentation of RBCs, and erythrophagocytosis. Of these, deformation and fragmentation of RBCs due to shearing, i.e., mechanical hemolysis, is the dominant mechanism of hemolysis in VADs. Mechanical hemolysis starts when an RBC deforms excessively in response to high shearing, and leaks part of its hemoglobin content into the bloodstream through small reversible openings in its membrane. Catastrophic hemolysis occurs when the RBC membrane ruptures. For over four decades, steady-shear hemolysis studies have been performed to understand mechanical hemolysis (17–20). Some of the early studies advocated the importance of wall shear stress and wall area (21), but it is well accepted now that mechanical hemolysis is primarily a bulk phenomenon, which depends on the shear stress and

exposure time (16,22). Although most studies of mechanical hemolysis have focused on the effects of steady shearing, a few unsteady-shearing experiments have also been reported (23).

Despite extensive experimentation, there is a lack of consensus on a model for mechanical hemolysis. Moreover, the timescale of most reported mechanical hemolysis experiments was three orders of magnitude greater than the timescale in a VAD. The typical flow rate in a VAD matches that of a human heart (5 L/min); the characteristic residence time of an RBC in a VAD is approximately 500 ms. Thus, most steady shear hemolysis data cannot be used for developing a blood damage model for VAD applications. Heuser and Opitz developed a Couette viscometer to measure hemolysis at short exposure times (24), and human-blood hemolysis experimental data from this setup were reported by Wurzinger et al. (25). Giersiepen et al. (26) developed a correlation (discussed below) for steady shear hemolysis based on these experiments. These hemolysis data and correlation are the most relevant for VAD applications, and are used here for developing a blood damage model.

Whereas the hemolysis experimental data are for steady shear loading, the flow in VADs is 3-dimensional and unsteady. Previous works attempted to relate the 3-dimensional flow effects to steady shear loading through a single scalar parameter. A few scalar-parameter-based hemolysis models have appeared in the literature over the past decade (e.g., Bludszuweit proposed a representative instantaneous one-dimensional stress parameter obtained from the six components of the deviatoric stress tensor) (27). These models relating the complex VAD flow to steady shear flows through a representative instantaneous scalar stress parameter for hemolysis prediction are hereafter called "stress-based" and are further discussed below. It is also important to note that the instantaneous stress, or instantaneous strain, models assume an instantaneous one-to-one relationship between local stress and RBC deformation; such relationship holds only in Lagrangian steady flows, i.e., flows where the velocity gradient is constant along streamlines (e.g., steady shear flow). The RBC membrane is viscoelastic, and the viscoelastic lag of blood cell membrane to the applied shear rate can be taken into account by considering accumulated straining. Another concern in the long term use of VADs is the repeated exposure to mechanical straining of the RBCs flowing through VAD implanted circulation. Yeleswarapu et al. developed a scalar damage accumulation model which incorporates the aging of RBCs (28). This model requires a damage function, which is unknown in complex flow situations. Thus, short exposure instantaneous stress-based models are presently used for hemolysis predictions.

GOVERNING EQUATIONS FOR BLOOD FLOW

Blood flow is modeled by the momentum and mass conservation equations for an incompressible fluid,

$$\rho\left(\frac{\partial \mathbf{u}}{\partial t} + \mathbf{u}\cdot\nabla\mathbf{u} - \mathbf{f}\right) = -\nabla p + \nabla\cdot\boldsymbol{\sigma}, \quad (1)$$

$$\nabla\cdot\mathbf{u} = 0 \quad (2)$$

where ρ is the blood density (1058 kg/m^3), $\mathbf{u}$ is the velocity, p is the pressure, $\boldsymbol{\sigma}$ is the extra stress, and $\mathbf{f}$ denotes body forces per unit mass (e.g., gravity). The problem is closed by prescribing an appropriate constitutive equation for the stress. Blood is a shear-thinning viscoelastic fluid; Yeleswarapu et al. showed that a generalized Oldroyd-B constitutive equation can describe well the rheological behavior of blood in shear flows (29). In the current work, we treat blood as a Newtonian liquid:

$$\boldsymbol{\sigma} = \mu(\nabla\mathbf{u} + \nabla\mathbf{u}^T), \quad (3)$$

where μ is dynamic viscosity of blood at high shear rate i.e., 3.5 mPa·s (cP). Thus, Eqs. 1 and 2 reduce to the incompressible Navier–Stokes equations. However, we develop the hemolysis model in a general context that can be applied to flow calculations performed with other constitutive models.

RED BLOOD CELLS IN SHEAR FLOW AND HEMOLYSIS

A blood damage model based on RBC deformation should account for RBC properties and deformation in shear flow, and it should be related to a relevant hemolysis data set. An RBC at rest is a biconcave disc of a viscoelastic membrane filled with a Newtonian liquid with a viscosity of approximately 6 mPa·s (cP). The RBC membrane has a relaxation time of approximately 200 ms which depends on the age of the cell (30), and it can support an estimated areal strain of 6% before rupturing (16). Owing to its biconcave shape, an RBC has 40% excess surface area compared to a sphere of the same volume. The excess surface area enables RBCs to undergo deformations that preserve both volume and surface area. In a flow, the RBCs behave as neutrally buoyant microcapsules with high deformabilty but small areal stretchability (31,32). The RBCs at rest aggregate into coinstack shaped structures called rouleaux. These structures break as shear stress increases, and RBCs become dispersed. As reported by Schmid-

Schönbein and Wells (31), the dispersed RBCs preserve their biconcave shape and tumble in a flow with shear stress below ≈ 0.1 Pa. The tumbling gradually reduces and the cells begin to align with the flow at ≈ 0.2 Pa. The RBCs deform into ellipsoidal shape, orient with the flow and show tank-treading at shear stress greater than 1 Pa. Tank-treading is a phenomenon in which the cell membrane rotates around the enclosed fluid. It is not clear if the RBCs deform into prolate or general ellipsoids, but most experimental studies refer to the general ellipsoidal state. The tank-treading and deformation into ellipsoidal shape has been confirmed in several later experimental studies (17,33). Leverett et al. found that above 150 Pa, extensive hemolysis occurs due to shear stress alone (19). This shear stress corresponds to shear rate of ≈ 42 000 s^{-1} for whole blood. The RBC membrane is believed to reach its 6% areal strain limit at this shear rate, so that any further stretching of the membrane leads to catastrophic hemolysis. Figure 1 (top) shows these configurations of RBC in shear flow. The leftmost state corresponds to no shear and shows rouleaux, and the rightmost state shows a hemolyzing RBC with pores on the surface.

Giersiepen et al. developed a correlation for steady-shear hemolysis at short time scales relevant to flow in a VAD based on experimental results by Wurzinger et al. (25,26). The correlation is:

$$\frac{\Delta Hb}{Hb} = 3.62 \times 10^{-7} \sigma^{2.416} \Delta t^{0.785}, \qquad (4)$$

where $\Delta Hb/Hb$ is the ratio of plasma free hemoglobin to the total hemoglobin in the sample (i.e., the plasma free hemoglobin plus hemoglobin enclosed in RBCs), σ is the shear stress (Pa) and Δt is exposure time (s). A plot of percentage hemolysis versus applied shear stress and exposure time is shown in Fig. 2(a). These physical properties, deformation configurations, and hemolysis data are used hereafter for developing the deformation based blood damage model.

Hemolysis predictions based on Eq. 4 have been recently reported for rotary blood pumps (34–36). De Wachter and Verdock used Eq. 4 to calculate hemolysis in hemodialysis cannulae (37). In these studies, the rate of hemolysis is integrated along the pathlines with an instantaneous scalar measure of stress σ to compute accumulated hemolysis. The rate of hemolysis,

$$\frac{d}{dt}\left(\frac{\Delta Hb}{Hb}\right) = 2.8417 \times 10^{-7} \sigma^{2.416} \Delta t^{-0.215}, \qquad (5)$$

is shown in Fig. 2(b). The hemolysis accumulation decreases with exposure time. It is important to note that the correlation (4) was developed in steady shear hemolysis experiments, where the shear stress σ is time independent: however, later studies of blood pumps used in Eq. 5 a scalar quantity derived from the instantaneous deviatoric stress tensor, $\sigma = \sqrt{-\frac{1}{2}\boldsymbol{\sigma} : \boldsymbol{\sigma}}$. As mentioned before, this method of computing hemolysis is here called "stress-based." While $\Delta Hb/Hb$ has been the measure of choice in all the above mentioned works, Normalized Index of Hemolysis (NIH) is the standard clinical index used

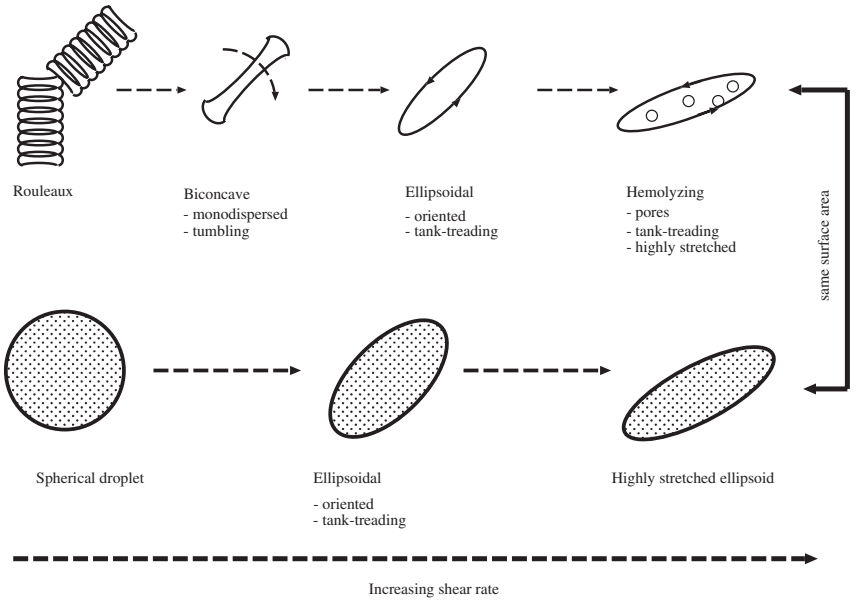

FIG. 1. Red blood cell and droplet deformation in shear flow: (top row) configurations of RBCs in increasing shear flow; (bottom row) spherical droplet deforming into a general ellipsoid.

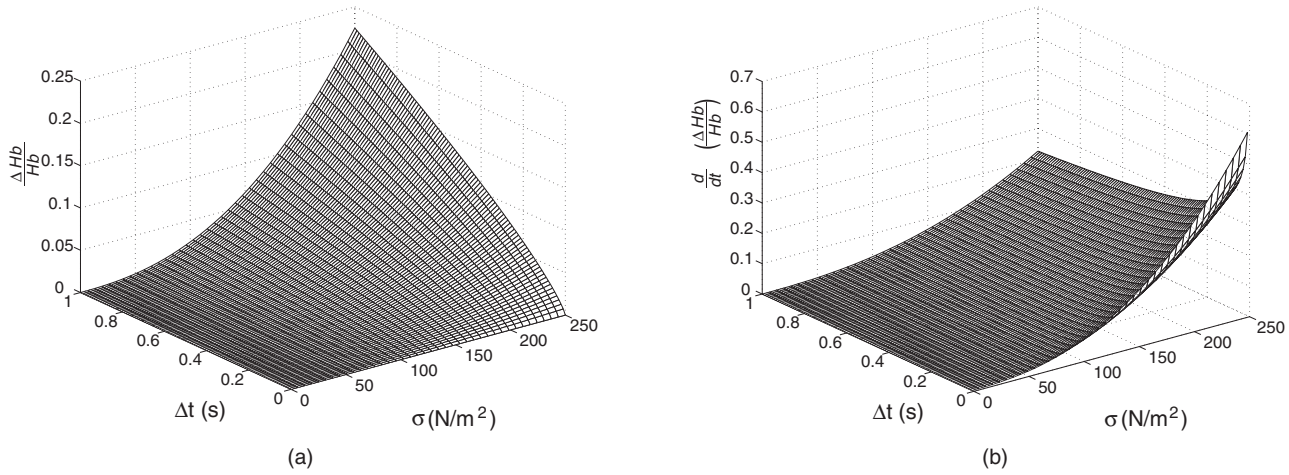

FIG. 2. Hemolysis correlation by Giersiepen et al. (26): (a) hemolysis versus exposure time Δt and stress σ; (b) rate of change of hemolysis correlation given by Eq. 5.

to report hemolysis (38) in flow loop tests. The NIH per single pass through a test loop is related to $\Delta Hb/Hb$ as:

$$\text{NIH}\ (g/100\ \text{L blood}) = 100 \times \frac{\Delta Hb}{Hb} \times (1 - Hct) \times \kappa, \tag{6}$$

where Hct is the blood hematocrit (45% for a healthy person) and κ is the hemoglobin content of blood (150 g/L for a healthy person). In this work both $\Delta Hb/Hb$ and NIH values are reported.

TENSOR-BASED MODEL OF RED BLOOD CELL DEFORMATION

An RBC in a general flow can be approximately viewed as a neutrally buoyant liquid droplet (31). Thus, the deformation of an RBC in shear flow can be approximated by that of a liquid droplet, by taking the physical properties of an RBC into consideration. This approach has been followed by Barthès-Biesel and Rallison (39), who derived a constitutive equation for the deformation of a droplet by balancing the interfacial tension with fluid stresses on either side of the interface. Maffettone and Minale proposed a droplet deformation equation in terms of a symmetric, positive-definite morphology tensor **S** that represents the shape of the droplet (40). The equation takes into consideration the competing action of interfacial tension on the droplet surface, which recovers the spherical shape of the droplet, and the force exerted by the surrounding liquid. The equation is frame-invariant (which makes it applicable to complex flows), and it accounts for nonaffine droplet deformation. Though RBCs can be modeled as droplets, the tank-treading motion shown by RBCs is absent in droplets. On the fluid interface of a droplet the internal and external fluid velocities match. For an RBC with tank-treading motion, the interface is a lipid bilayer that rotates around the enclosed liquid with a velocity proportional to the local fluid shear rate (33); the local velocities of both internal and external fluids match the rotation velocity of the membrane. In what follows, we modify the original equation to account for the tank-treading phenomenon peculiar to RBCs in shear flow, while preserving the frame invariance.

Consider a general flow with velocity gradient $\nabla\mathbf{u}$. The velocity gradient can be decomposed into the symmetric rate of strain tensor **E** and the antisymmetric vorticity tensor **W**, as:

$$\nabla\mathbf{u} = \mathbf{E} + \mathbf{W}; \quad \mathbf{E} = \frac{1}{2}(\nabla\mathbf{u} + \nabla\mathbf{u}^T); \quad \mathbf{W} = \frac{1}{2}(\nabla\mathbf{u} - \nabla\mathbf{u}^T). \tag{7}$$

The droplet deformation equation as proposed by Maffettone and Minale (40) is:

$$\mathbf{S}^{\circ} = f_2\,[\mathbf{E}\cdot\mathbf{S} + \mathbf{S}\cdot\mathbf{E}] - f_1\,[\mathbf{S} - g(\mathbf{S})\mathbf{I}], \tag{8}$$

where

$$g(\mathbf{S}) = \frac{3III}{II}, \tag{9}$$

and II and III are second and third invariants of **S**, respectively, defined as:

$$II = \frac{1}{2}\left(\text{tr}(\mathbf{S})^2 - \text{tr}(\mathbf{S}^2)\right); \quad III = \det(\mathbf{S}). \tag{10}$$

The parameters f_1 and f_2 depend on the physical properties of the liquid droplet. The first term on the right-hand side represents how the flow acts to deform the droplet, and the second term accounts for

the resisting effect of interfacial tension. The left-hand side term,

$$\mathbf{S}^{\circ} \equiv \frac{d\mathbf{S}}{dt} - [\mathbf{W}\cdot\mathbf{S} - \mathbf{S}\cdot\mathbf{W}]; \quad \frac{d\mathbf{S}}{dt} = \frac{\partial \mathbf{S}}{\partial t} + \mathbf{u}\cdot\nabla\mathbf{S}, \quad (11)$$

represents the Jaumann derivative, and indicates that the droplet is rotating with the vorticity of the external fluid. This term makes the equation frame-invariant. Roscoe showed that for a tank-treading ellipsoidal particle the effective vorticity seen by the particle reduces in proportion to the tank-treading frequency (41). This result holds true for a stationary ellipsoid that maintains a fixed orientation with the flow. A tank-treading ellipsoidal RBC in unsteady flow has varying orientation with the flow, and only sees a reduction in relative vorticity, i.e., the difference between the vorticity **W** and the rate of rotation of the principal axes of the ellipsoidal particle. The relative vorticity becomes apparent, if we consider an orthogonal frame of reference rotating with respect to the fixed orthonormal frame as:

$$\tilde{\mathbf{e}}_i = \mathbf{Q}(t)\cdot\mathbf{e}_i, \quad (12)$$

where $\mathbf{e}_i$ and $\tilde{\mathbf{e}}_i$ are the orthonormal vectors of fixed and rotating frames, and **Q** is the volume-preserving rotation matrix ($\mathbf{Q}\cdot\mathbf{Q}^T = \mathbf{I}$). The velocity gradients in the two frames are related as:

$$\tilde{\nabla}\tilde{\mathbf{v}} = \nabla\mathbf{v} + \dot{\mathbf{Q}}^T\cdot\mathbf{Q}. \quad (13)$$

This can also be written as:

$$(\tilde{\mathbf{E}} + \tilde{\mathbf{W}}) = (\mathbf{E} + \mathbf{W}) + \dot{\mathbf{Q}}^T\cdot\mathbf{Q}. \quad (14)$$

Since $\dot{\mathbf{Q}}^T\cdot\mathbf{Q}$ is a skew symmetric tensor, taking transpose of the above equation, and adding and subtracting to itself we get:

$$\tilde{\mathbf{E}} = \mathbf{E}; \quad \tilde{\mathbf{W}} = \mathbf{W} + \dot{\mathbf{Q}}^T\cdot\mathbf{Q} \equiv \mathbf{W} - \boldsymbol{\Omega}, \quad (15)$$

where $-\boldsymbol{\Omega} = \dot{\mathbf{Q}}^T\cdot\mathbf{Q}$ is the rotation rate of the rotating frame with respect to the fixed one. To account for the instantaneous rotation of the tank-treading cell we consider the rotating frame defined by the unit eigenvectors $\tilde{\mathbf{e}}_i$ of **S**; the rotation $\boldsymbol{\Omega}$ is hence computed as:

$$\boldsymbol{\Omega} = \tilde{\mathbf{e}}_i\frac{d\tilde{\mathbf{e}}_i}{dt} = \tilde{\mathbf{e}}_i\left(\frac{\partial\tilde{\mathbf{e}}_i}{\partial t} + \mathbf{u}\cdot\nabla\tilde{\mathbf{e}}_i\right). \quad (16)$$

Thus, Maffettone and Minale (40) equation of droplet deformation in a frame of reference rotating with the cell becomes:

$$\mathbf{S}^{\circ} = -f_1[\mathbf{S} - g(\mathbf{S})\mathbf{I}] + f_2[\tilde{\mathbf{E}}\cdot\mathbf{S} + \mathbf{S}\cdot\tilde{\mathbf{E}}] + f_3[\tilde{\mathbf{W}}\cdot\mathbf{S} - \mathbf{S}\cdot\tilde{\mathbf{W}}], \quad (17)$$

where

$$\mathbf{S}^{\circ} \equiv \frac{d\mathbf{S}}{dt} - [\boldsymbol{\Omega}\cdot\mathbf{S} - \mathbf{S}\cdot\boldsymbol{\Omega}]. \quad (18)$$

It is assumed that the shape of the droplet remains ellipsoidal at all times. It can be easily verified that Eq. 17 preserves the volume of the droplet (i.e., $dIII/dt = 0$). The first term on the righthand side of Eq. 17 models the shape recovery of the droplet in the absence of shear stress. The second term represents the nonaffine deformation of the droplet, and the third term accounts for the tank-treading motion which reduces the relative vorticity seen by the droplet. Such reduction in vorticity was also applied to RBCs by Keller and Skalak, while keeping the RBC at a fixed orientation (42). The eigenvalues of **S** are the square lengths of the three axes of the shape ellipsoid. Equation 17 is an implicit equation in **S** because the rotation rate $\boldsymbol{\Omega}$ depends on **S** (unless the flow is steady, where $d\mathbf{S}/dt = 0$ and $\boldsymbol{\Omega} = 0$). Figure 1 (bottom) shows the deformed droplet configuration as represented by our model in comparison to the actual shape of a deformed RBC in shear flow. The droplet is spherical at no shear ($\mathbf{S} = \mathbf{I}$), and becomes ellipsoidal as the shear increases. The ellipsoidal shape and orientation is identified by the eigenvalues of **S**.

PARAMETERS

Equation 17, in its general form, is applicable to a microcapsule that shows tank-treading. The equation is made specific for capturing RBC deformation by setting its parameters f_1, f_2, and f_3. The steady shear experimental observations reported in the literature are used to choose the appropriate values of these parameters. In the absence of flow, a deformed droplet relaxes to its natural configuration according to:

$$\frac{d\mathbf{S}}{dt} = -f_1(\mathbf{S} - g(\mathbf{S})\mathbf{I}). \quad (19)$$

For small deformations $\mathbf{S} \approx \mathbf{I} + \varepsilon\mathbf{A}$; consequently, Eq. 19 reduces to $d\mathbf{A}/dt = -f_1\mathbf{A}$ (Appendix A). The solution to this approximate equation is $\mathbf{S} = \mathbf{I} + \varepsilon\mathbf{A}_0\exp(-f_1 t)$, and has $1/f_1$ as the relaxation time. The relaxation time of RBCs is approximately 200 ms (30). Thus, we set:

$$f_1 = 5.0\ \mathrm{s}^{-1}, \quad (20)$$

so that the droplet and the RBC have the same relaxation time. It is important to note that, although droplets and RBCs recover to different shapes, they both deform into ellipsoidal shapes under shearing.

In Eq. 17, the eigenvalues of the morphology tensor show oscillatory transients at varying shear rates when $f_2 \neq f_3$. Such shape fluctuations have not been

observed experimentally; thus, we restrict $f_2 = f_3$. In a steady shear flow,

$$\nabla \mathbf{u} = \begin{bmatrix} 0 & G & 0 \\ 0 & 0 & 0 \\ 0 & 0 & 0 \end{bmatrix} = \underbrace{\begin{bmatrix} 0 & G/2 & 0 \\ G/2 & 0 & 0 \\ 0 & 0 & 0 \end{bmatrix}}_{\mathbf{E}} + \underbrace{\begin{bmatrix} 0 & G/2 & 0 \\ -G/2 & 0 & 0 \\ 0 & 0 & 0 \end{bmatrix}}_{\mathbf{W}}, \tag{21}$$

where G is the intensity of the flow. At steady state, the droplet remains at fixed orientation to the flow ($\mathbf{\Omega} = 0$), and the steady-state droplet deformation equation is:

$$f_1 = (\mathbf{S} - g(\mathbf{S})\mathbf{I}) = f_2(\nabla \mathbf{u} \cdot \mathbf{S} + \mathbf{S} \cdot \nabla \mathbf{u}^T). \tag{22}$$

The eigenvalues λ_1, λ_2, and λ_3 of S are computed straightforwardly from Eq. 22 as:

$$W^2 = \lambda_1 = \left(\frac{f_1^2}{f_1^2 + f_2^2 G^2} \right)^{1/3}, \tag{23}$$

$$L^2 = \lambda_2 = \left(\frac{f_1^2}{f_1^2 + f_2^2 G^2} \right)^{1/3} \left[\frac{(f_1^2 + f_2^2 G^2) + G f_2 \sqrt{f_1^2 + f_2^2 G^2}}{f_1^2} \right], \tag{24}$$

$$B^2 = \lambda_3 = \left(\frac{f_1^2}{f_1^2 + f_2^2 G^2} \right)^{1/3} \left[\frac{(f_1^2 + f_2^2 G^2) - G f_2 \sqrt{f_1^2 + f_2^2 G^2}}{f_1^2} \right], \tag{25}$$

where L, B, and W are three semiaxial lengths of the droplet. The major axis of the droplet is oriented to the flow at an angle:

$$\theta = \tan^{-1}\left(\frac{f_1}{G f_2 + \sqrt{G^2 f_2^2 + f_1^2}} \right). \tag{26}$$

As shown in the rightmost states of Fig. 1 (bottom), the droplet surface area is matched with the hemolyzing RBC (6% areal strain at 42 000 s^{-1}). The area of a general ellipsoidal droplet is computed by a convergent series used by Keller and Skalak (42). An undeformed RBC has 40% excess surface area with respect to a droplet of same volume, and it undergoes 6% areal strain before hemolyzing; therefore, an ellipsoidal droplet such as that used in our model with the same volume as an RBC should stretch to 1.4×1.06 times its original surface area at "hemolysis." Matching the droplet area with hemolyzing RBC area gives:

$$f_2 = f_3 = 1.25 \times 10^{-3}. \tag{27}$$

Thus, the three parameters f_1, f_2, and f_3 together incorporate relaxation time, long-lived shape oscillations, tank-treading, and critical areal strain limit into the hemolysis model. Equation 17, with these parameter values, can be used to estimate RBC deformation in a general flow.

HEMOLYSIS PREDICTION

In a strain-based hemolysis model, it is reasonable to assume that the instantaneous rate of leaking of hemoglobin through an RBC membrane—i.e., the rate of hemolysis—depends on the instantaneous shape distortion of the RBC. Equation 17 gives the instantaneous shape of the droplet in a general flow; the instantaneous shape distortion $D = (L - B)/(L + B)$ is computed using the axial lengths of the droplet (the eigenvalues of **S**). In a steady shear flow there is a unique relationship between the distortion and the intensity G_{eff}, as well as the corresponding steady shear stress σ_{eff} Equations 23–25 yield:

$$G_{\text{eff}} = \sqrt{\frac{f_1^2 D^2}{(1 - D^2) f_2^2}}, \tag{28}$$

$$\sigma_{\text{eff}} = \mu_{\text{blood}}\, G_{\text{eff}}. \tag{29}$$

Because in steady shear there is a one-to-one correspondence of shear stress and distortion, we construct a strain-based hemolysis model by requiring that the strain-based and stress-based models yield the same results in steady shearing; using Eq. 4 as in the stress-based model, results in a strain-based relationship:

$$\frac{\Delta Hb}{Hb} = 3.62 \times 10^{-7} \left(\mu_{\text{blood}} \sqrt{\frac{f_1^2 D^2}{(1 - D^2) f_2^2}} \right)^{2.416} t^{0.785}. \tag{30}$$

Below, we compare the strain-based and stress-based hemolysis prediction for homogeneous and inhomogeneous flows, after discussing the numerical aspects.

NUMERICAL METHOD

The blood flow in a complex domain is obtained by solving the governing equations with the stabilized space-time finite element method, and the moving boundaries are handled with a sliding mesh technique. A complete description of the finite element method for 3-dimensional analysis of the Gyro centrifugal blood pump has been previously reported (3,4). The velocity and pressure data from the CFD simulation are postprocessed to obtain RBC deformation.

A least-squares recovery procedure is used to extract accurate velocity gradients from the velocity data. In the case of a general inhomogeneous flow, the RBC deformation is computed along pathlines. This enables a Lagrangian computation of RBC morphology given by Eq. 17 The coordinates of pathlines are computed using forward Euler integration as:

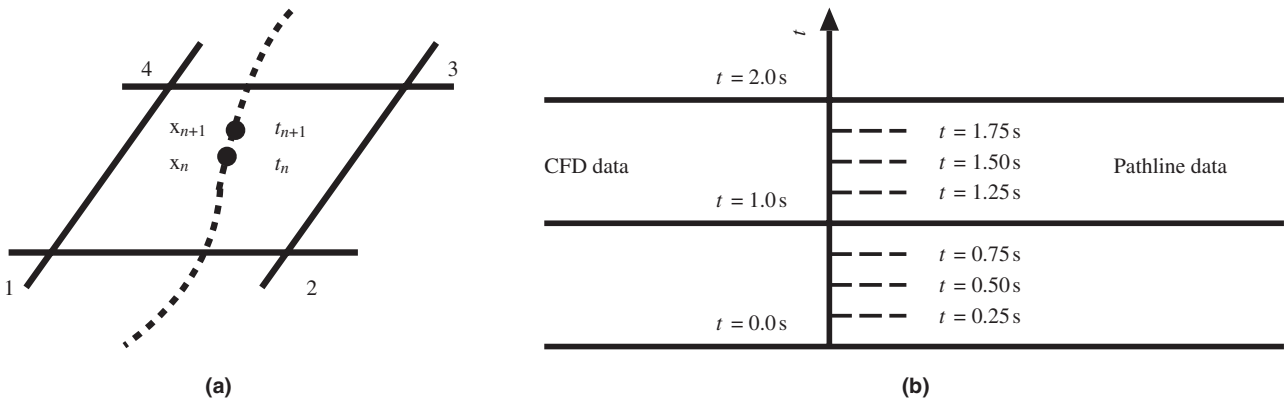

FIG. 3. Interpolation of velocity data: (a) spatial interpolation—the dotted line represents a pathline running through an element; (b) temporal interpolation—pathline data in the right are interpolated from CFD data on the left.

$$\mathbf{x}_{n+1} = \mathbf{x}_n + \mathbf{u}_n \Delta t, \tag{31}$$

where n is the temporal index of the trace point, and $\mathbf{x}_n$ and $\mathbf{x}_{n+1}$ are positions of the trace point at time t_n and $t_{n+1} = t_n + \Delta t$, respectively. Figure 3(a) shows two trace points, $\mathbf{x}_n$ and $\mathbf{x}_{n+1}$, inside an element formed by mesh nodes—1, 2, 3, and 4. The velocity $\mathbf{u}_n$ is interpolated at location $\mathbf{x}_n$ using piecewise linear shape functions over the finite element mesh. Unlike in a steady problem, velocity data in unsteady cases are available only at discrete time-steps. For accurate pathline tracing, the step-ratio (ratio of step size $|\mathbf{x}_{n+1} - \mathbf{x}_n|$ to maximum velocity $|\mathbf{u}|_{\max}$ in the domain) is set to ~10^{-5}. Due to such a small step-ratio, the number of trace points along the pathline is much larger than the number of discrete time steps of the CFD data. The data between CFD time-steps are interpolated linearly to obtain velocities at the pathline time-steps. Figure 3(b) shows the temporal discretization with CFD data on the left and pathline steps on the right. Thus, both spatial and temporal interpolations are required for the unsteady problems whereas only spatial interpolation is required for the steady cases.

The droplet morphology is also solved using forward Euler integration along a pathline as:

$$\mathbf{S}_{n+1} = \mathbf{S}_n + \Delta \mathbf{S}_n, \tag{32}$$

$$\Delta \mathbf{S}_n = \left(-f_1[\mathbf{S}_n - g(\mathbf{S}_n)\mathbf{I}] + f_2[\tilde{\mathbf{E}}_n \cdot \mathbf{S}_n + \mathbf{S}_n \cdot \tilde{\mathbf{E}}_n] + f_3[\tilde{\mathbf{W}}_n \cdot \mathbf{S}_n - \mathbf{S}_n \cdot \tilde{\mathbf{W}}_n] + [\mathbf{\Omega}_n \cdot \mathbf{S}_n - \mathbf{S}_n \cdot \mathbf{\Omega}_n]\right)\Delta t. \tag{33}$$

All the n^{th} quantities are computed at t_n. Unlike the rate of strain and vorticity tensors, the rotation rate tensor $\mathbf{\Omega}_n$ is computed using the information from the $(n-1)^{\text{th}}$ step:

$$\mathbf{\Omega}_n = \sum_i (\mathbf{e}_i)_n \frac{(\mathbf{e}_i)_n - (\mathbf{e}_i)_{n-1}}{\Delta t}, \tag{34}$$

where $(\mathbf{e}_i)_n$ and $(\mathbf{e}_i)_{n-1}$ are eigenvectors of $\mathbf{S}_n$ and $\mathbf{S}_{n-1}$, respectively. The orientation of the eigenvectors is checked at each step to ensure correct computation of the rotation rate.

An instantaneous distortion D_n is computed from the eigenvalues of $\mathbf{S}_n$, and is used to compute an equivalent effective steady shear flow intensity $(G_{\text{eff}})_n$ and shear stress $(\sigma_{\text{eff}})_n$. Hemolysis accumulated along the pathlines is computed by integrating the rate of hemolysis correlation in Eq. 5.

In the case of homogeneous shear flows, the rate of strain and vorticity tensors are known analytically; thus, the equation can be simply integrated without tracing pathlines. In the next section we consider homogeneous steady and sinusoidal shear flows, and an inhomogeneous flow in a 2-dimensional blood pump.

NUMERICAL RESULTS

Steady shear flow

For steady shear flow of intensity G, the velocity gradient and droplet deformation are given by Eqs. 21 and 22, respectively. The eigenvalues computed in Eqs. 23–25 are used to compute the distortion D, which when used in Eq. 28 gives:

$$G_{\text{eff}} = G; \quad \sigma_{\text{eff}} = \sigma, \tag{35}$$

as expected. Because the effective membrane stress is the same as the fluid stress, the hemolysis prediction by both stress- and strain-based models match exactly in a steady shear flow. For example, both stress- and strain-based hemolysis models predict $\Delta Hb/Hb = 0.306\%$ for $G = 5000\ \text{s}^{-1}$ after 15 s.

Sinusoidal shear

Consider a steady shearing flow of intensity G_o superimposed with sinusoidal shearing $G_1 \sin(\omega t)$. The intensity $G(t)$ of the model flow is:

$$G(t) \equiv \frac{du_x}{dy} \equiv G_0 + G_1 \sin(\omega t). \quad (36)$$

A similar flow is observed in VADs, where baseline shearing is superimposed with a periodic impulse caused by rotating impeller or a pulsating chamber. Such a flow may also be observed for devices connected to the heart. Since the model flow is homogeneous and the velocity gradient is known, we can integrate Eq. 17 in a Lagrangian frame by the explicit Euler method to get the morphology tensor **S**.

To study hemolysis in the case of sinusoidal shearing we define 3 nondimensional parameters:

$$\alpha = G_0 f_2 \tau, \quad (37)$$

$$\beta = \frac{G_1}{G_0}, \quad (38)$$

$$\gamma = \omega\tau, \quad (39)$$

where τ is the relaxation time of RBC membrane (200 ms), α is a measure of baseline shearing, β is the strength of sinusoidal pulse, and γ is the nondimensional frequency. To account properly for the effect of exposure time we compute the hemolysis accumulated in 20 s of shearing after steady state is achieved. A range of α, β, and γ is selected and hemolysis response is studied. The nondimensional frequency γ is varied from 0.4 to 10, such that there are enough cycles in 20 s at the lowest frequency. The range of α and β ensure that the maximum shear rate never exceeds the critical strain rate limit of 42 000 s^{-1}. As expected, the hemolysis scales as:

$$\frac{\Delta Hb}{Hb} \propto \alpha^{2.416}, \quad (40)$$

over the complete range of α, i.e., the effect of the baseline shearing in a superimposed steady plus sinusoidal shearing flow is the same as the effect of the constant shearing in a steady shearing flow. Figure 4 shows a plot of percentage $(\Delta Hb/Hb)/\alpha^{2.416}$ versus β and γ.

For $\gamma < 1.0$, i.e., for a low frequency sinusoidal impulse, the time period of the sinusoidal shearing is comparable to the relaxation time of RBC. Thus, the cell deformation closely follows the sinusoidal shearing, and the effective stress σ_{eff} closely matches the instantaneous fluid shear stress σ. As a result, both stress- and strain-based models predict similar levels of hemolysis, and match each other exactly as γ tends to zero (which corresponds to the steady shear case). As the frequency increases, the time period of sinusoidal shearing becomes smaller than the RBC relaxation time. Consequently, the RBC does not deform completely in response to rapidly varying sinusoidal shearing. Thus, the contribution of the sinusoidal component of shearing to the cell deformation diminishes with increasing frequency. This result is consistent with Hashimoto's experimental observation of decrease in RBC destruction when exposure time at larger shear rate (>500 s^{-1}) is interspersed with smaller shear rates (<300 s^{-1}) (23). For γ-value as high as 10, the time period of sinusoidal shearing is 20 ms, and the sinusoidal component of shearing does not cause any significant cell deformation. Consequently, the hemolysis is caused by the baseline shearing only.

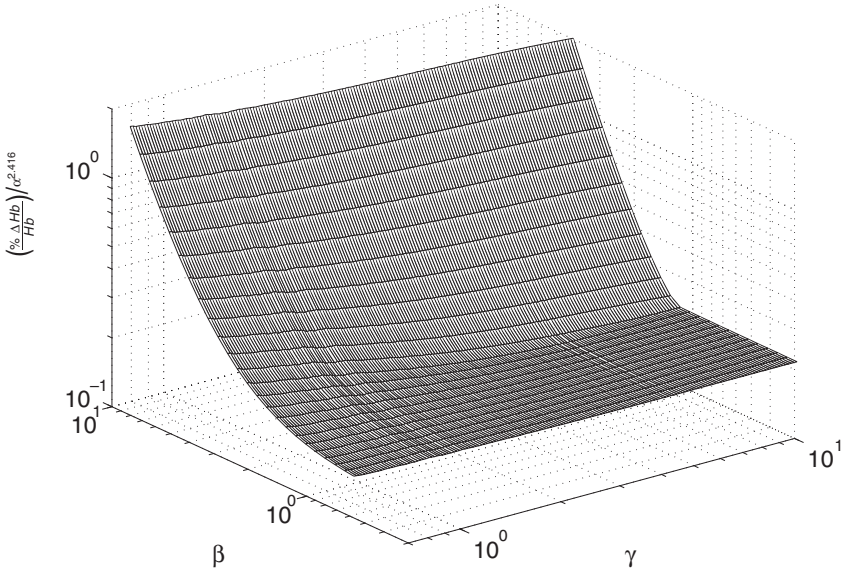

FIG. 4. Sinusoidal shear flow: % $(\Delta Hb/Hb)/\alpha^{2.416}$ versus β and γ.

The nondimensional amplitude of sinusoidal shearing β, determines the contribution of sinusoidal impulse to cell deformation. For $\beta < 1$, the predicted hemolysis grows with increasing β; as expected, this enhanced contribution to hemolysis is significant when $\gamma < 1$. As the magnitude of the fluctuating component of the shear rate approaches the baseline shearing value ($\beta \approx 1$) at low frequency ($\gamma < 1$), the cell deformation follows closely the sinusoidal shearing; thus, the cell shape oscillates between a completely relaxed state and a highly stretched one. A further increase in β causes a reversal in the deformation of the cell during part of the period of oscillation. This yields a higher predicted effective baseline shearing. While the effect of flow reversal, i.e., $\beta > 1$, and consequent increase in baseline shearing is gradual when $\gamma < 1$, there is a sharper increase when $\gamma > 1$.

These results indicate that a low baseline shearing with superimposed high frequency (or short-lived) spikes is less damaging than a constant shearing of intermediate intensity. In the context of centrifugal devices, this suggests that conical centrifugal pumps with constant, uniform shear should yield higher hemolysis than vaned centrifugal pumps, where the blood cells experience short-lived high shear levels interspersed with low shear baseline values. This has also been found in recent experimental studies by Kawahito and Nosé (12). It is important to stress that the difference between hemolysis prediction with stress- and strain-based model increases with the frequency of the fluctuating shear component.

A particular case with $\alpha = 0.5$, $\beta = 0.75$ and $\gamma = 4$ is observed for 1 s, and shown in Fig. 5. The 1-s window of observation was selected only after the end of the transient response to sinusoidal shearing. Figure 5(a) shows the maximum eigenvalue λ_{max} of **S** and sinusoidal shear flow intensity $G(t)$ with respect to time. The eigenvalue lags the sinusoidal impulse due to the viscoelastic nature of the RBC. The phase difference between the sinusoidal shearing and the eigenvalue response is directly proportional to the sinusoidal frequency. Figure 5(b) shows the accumulated hemolysis as predicted by the strain- and stress-based models in the observed time period. The stress-based model assumes equivalence of the instantaneous fluid stress and RBC membrane stress. On the other hand, the strain-based model computes an equivalent steady shear stress corresponding to an RBC deformation. Hence, the stress-based model predicts higher hemolysis than the strain-based model. Both stress- and strain-based hemolysis predictions start from zero, but the stress-based hemolysis has a higher average slope than the strain-based model. Because over longer exposure times the average slope determines the hemolysis, the difference between the stress- and strain-based hemolysis increases with the exposure time. The accumulation of hemolysis over a period of 20 s is shown in Fig. 5(c).

Hemolysis in 2-dimensional pump

The steady and sinusoidal shearing experiments involve homogeneous simple shear flows; the flow in VADs is inhomogeneous and 3-dimensional. A simplified 2-dimensional version of the 3-dimensional Gyro centrifugal blood pump (43) is constructed to test the hemolysis model. Figure 6(a) shows the geometry of the blood pump. It has a chamber diameter of 5.6 cm, and inlet and outlet ports are 0.8 cm in width. A 4-vane impeller rotates at 600 rpm and the flow rate (per unit depth) in the pump is 2.59 (L/cm)/min. The geometric parameters and flow rate are similar to the Gyro operating conditions. Specifically, the flow rate is chosen so that the average residence time of a blood cell traveling through the 2-dimensional blood pump is the same as the typical

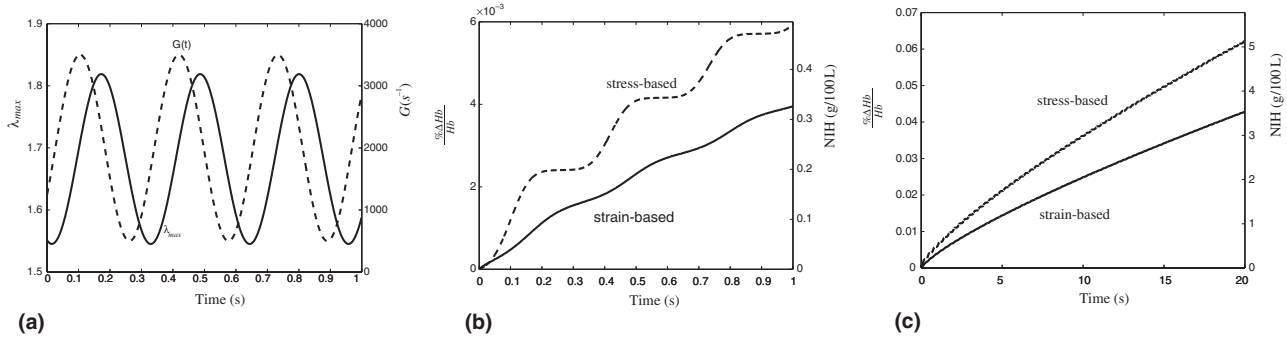

FIG. 5. Sinusoidal shear flow ($G_0 = 2000\ s^{-1}$; $G_1 = 1500\ s^{-1}$; $\omega = 20\ s^{-1}$): (a) maximum eigenvalue and flow intensity versus time ($f_1 = 5/s$, $f_2 = f_3 = 1.25 \times 10^{-3}$); (b) stress- and strain-based hemolysis accumulation versus observation time of 1 s; (c) stress- and strain-based hemolysis accumulation versus observation time of 20 s.

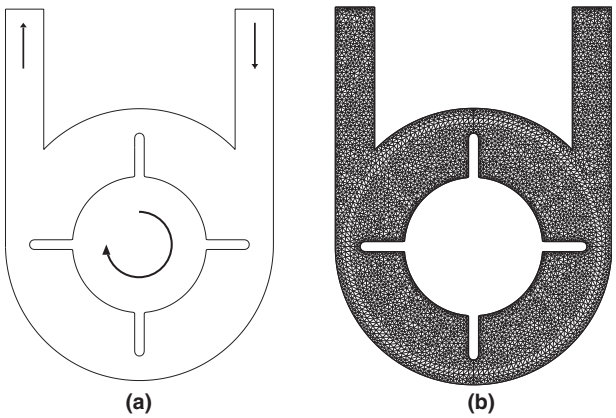

FIG. 6. Two-dimensional pump: (a) geometry; (b) hybrid mesh.

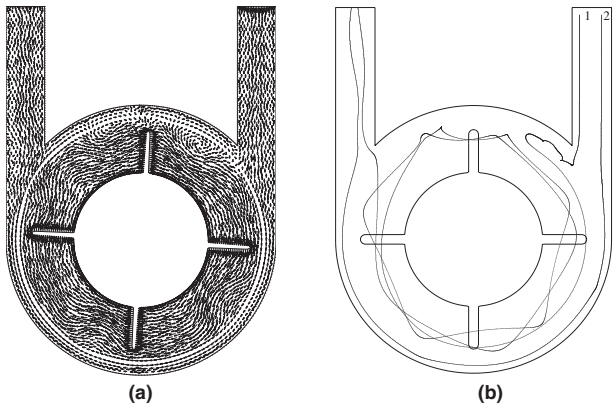

FIG. 7. Two-dimensional pump: (a) velocity after 10 revolutions; (b) pathlines.

residence time in the Gyro blood pump operating under normal conditions; the range of shear rates is comparable.

Figure 6(b) shows the structured/unstructured finite element mesh, with 10 506 nodes and 9498 elements. A moving unstructured mesh is attached to the impeller, and another stationary mesh is attached to the chamber walls. These two unstructured meshes are stitched together with a structured mesh. The rotation of the impeller mesh is accommodated using the shear-slip mesh update method. The impeller completes one revolution in 160 time steps of 0.625 ms each. The velocity and pressure data are saved at every step. Figure 7(a) shows the velocity vectors in the pump after 10 revolutions. The droplet deformation along the pathlines is computed with the Euler integration scheme by our postprocessor. A piecewise linear interpolation of velocity is used over the finite element mesh to obtain the data at the trace points. Because the flow is unsteady, a linear interpolation in the temporal direction is also used to obtain the nodal velocities at the trace point time steps. The components of the velocity gradients are recovered by a least-squares recovery procedure at each trace point time step. Figure 7(b) shows two pathlines traced in the 2-dimensional pump flow using the velocity data. Figure 8 shows the changes in eigenvalues of the morphology tensor and the hemolysis prediction along these pathlines. As expected, the eigenvalue of the morphology tensor along the first pathline shows similarity between the sinusoidal shearing and 2-dimensional blood pump flow. The similarity is distinctly visible in the stress-based hemolysis predictions where the stress-based hemolysis characteristic along the first pathline is similar to the corresponding sinusoidal shearing flow. As in the case of sinusoidal shearing, the strain-based model predicts lower hemolysis than the stress-based one. This implies that the RBCs moving along these pathlines are affected by the baseline shearing only, and the short-lived high shear rates do not have any significant effect. We calculated the average hemolysis by scattering 100 uniformly distributed tracer points over the inflow section and following them for up to 1.0 s (or until they exit the device). The total average hemolysis computed with

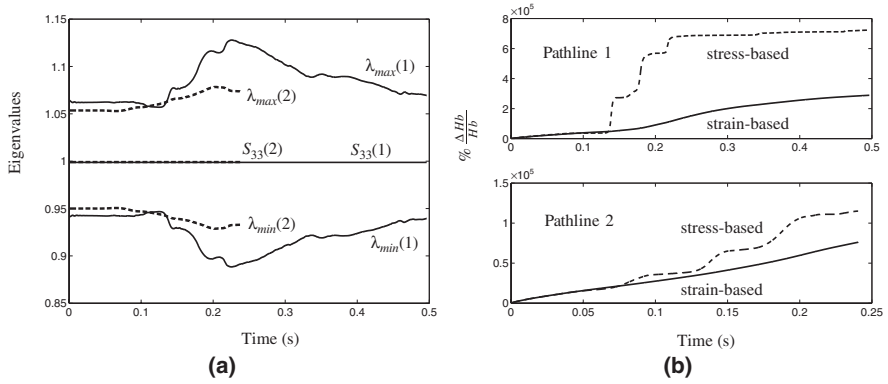

FIG. 8. Two-dimensional pump: (a) eigenvalue of morphology tensor; (b) hemolysis for two pathlines shown in Fig. 7(b).

the stress-based model is 2.01×10^{-5}% per trace point, whereas the hemolysis predicted by the strain-based model is 1.45×10^{-5}%. (By using Eq. 6 this can be translated to NIH values per single pass through the pump of 1.66×10^{-3} and 1.19×10^{-3} g/100 L for the stress-based and strain-based models, respectively; although the 2-dimensional pump is a hypothetical one, these values fall in the typical range for actual centrifugal blood pumps, e.g., 1×10^{-3} to 4×10^{-3} g/100 L) (12,44).

CONCLUSIONS

The design cycle of VADs can be considerably shortened by the use of CFD in the design process. CFD are frequently applied to obtain an appropriate flow rate, pressure head, velocity profile, etc., i.e., an efficient hydraulic design of VADs. However, predicting mechanical hemolysis levels—hematologic design—requires a realistic model for blood damage. The experimental research on mechanical hemolysis has focused mainly on steady shear flows, and a correlation is available for such experimental data relating hemolysis to exposure time and steady shear stress. In the absence of any unsteady data and correlation, CFD-based hemolysis predictions in the past have used the steady correlation directly in the unsteady flow situations by replacing the steady shear stress with a scalar quantity derived from the instantaneous deviatoric stress tensor. Such a method is here called "stress-based."

This work proposes a tensor-based blood damage model, also referred to as "strain-based" method. The model is developed using an analogy between RBCs and droplets. In the model, an instantaneous morphology of RBC is computed, which consequently provides an instantaneous deformation estimate of RBC. A steady shear stress corresponding to the instantaneous deformation is used in the steady shearing hemolysis correlation to predict hemolysis. The model incorporates experimentally observed phenomena—tank-treading and ellipsoidal deformation. The parameters of the model are set based on experimentally measured quantities—relaxation time of the RBC membrane, excess surface area of the RBC as compared to a droplet of the same volume, and the strain rate threshold for catastrophic hemolysis. The model also accounts for the estimated areal strain limit of the RBC membrane.

The strain-based model is tested in both homogeneous flows, where the velocity gradient is uniform throughout the flow domain, and inhomogeneous flows. The stress-based model of Giersiepen et al. (26) and the strain-based model proposed in this article predict equal hemolysis levels in steady simple shear flow and agree equally well with the data of Wurzinger et al. (25). The stress-based model predicts higher hemolysis when a sinusoidal shear flow is superimposed on a simple shear flow. This difference suggests that the relative merit of stress-based and strain-based models could be assessed by studying short-time hemolysis in flows where a time-periodic straining is superimposed on a steady straining; an apparatus for such studies could be built by modifying the flow-through Couette device of Heuser and Opitz (24) and driving the inner cylinder at a time-dependent rate.

The difference between the stress- and strain-based models grows as the frequency of sinusoidal shearing increases. This is consistent with the experimental observation of negligible hemolysis in a blood sample exposed for a few microseconds to shear stress as high as 1000 Pa (16). In the context of blood pumps, this suggests that sustained moderate levels of stress (typically encountered in conical blood pumps) may be more damaging than a short-lived high shear stresses superimposed on a lower baseline shearing (typically seen in vaned centrifugal blood pumps). The RBC deformation is computed in a 2-dimensional blood pump, and hemolysis predictions by the two models are compared along pathlines. The stress-based model predicts a higher hemolysis than the strain-based one. Albeit in a simplistic way, the strain-based model accounts for the physical phenomena of RBC membrane stretching and is thus a suitable candidate for realistic hemolysis predictions.

Currently, a 3-dimensional implementation of the deformation equation is under development; the results from a complete 3-dimensional blood-pump simulation will be compared with experiments being conducted at Baylor College of Medicine. Data from this study will further assess the model, and would be immensely valuable for VAD designers. The proposed model can also be used to optimize VAD design by minimizing the deviation of the morphology tensor from identity over a family of pathlines.

Acknowledgments: This work was supported by the National Science Foundation under award CTS-ITR-0312764, and by Texas ATP grant 003604-0011-2001. Computational Resources were provided by the National Partnership for Advanced Computational Infrastructure (NPACI), by the Rice Computational Engineering Cluster, funded by NSF through MRI award EIA-0116289, and by the Rice Terascale Cluster funded by NSF under Grant EIA-0216467, Intel, and Hewlett-Packard.

REFERENCES

1. DeBakey ME. The odyssey of the artificial heart. *Artif Organs* 2000;24:405–11.
2. Olsen DB. Presidential address: the history of continous-flow blood pumps. *Artif Organs* 2000;24:401–4.
3. Behr M. Biofluid simulations on Linux clusters. In: Matsuno K, Ecer A, Periaux J, Satofuka N, Fox P, eds. *Parallel Computational Fluid Dynamics—New Frontiers and Multi-Disciplinary Applications*. New York: Elsevier, 2003;451–8.
4. Behr M, Arora D. Shear-slip mesh update method: Implementation and applications. *Comput Methods Biomech Biomed Engin* 2003;6:113–23.
5. Anderson JB, Wood HG, Allaire PE, Bearnson G, Khanwilkar P. Computational flow study of the continuous flow ventricular assist device, prototype number 3 blood pump. *Artif Organs* 2000;24:377–85.
6. Miyazoe Y, Sawairi T, Ito K, et al. Computational fluid dynamic analysis to establish design process of centrifugal blood pumps. *Artif Organs* 1998;22:381–5.
7. Yu SCM, Ng BTH, Chan WK, Chau LP. The flow patterns within the impeller passage of a centrifugal blood pump model. *Med Engin Phys* 2000;22:381–93.
8. Qian Y, Bertram CD. Computational fluid dynamics analysis of hydrodynamic bearings of the ventrassist rotary blood pump. *Artif Organs* 2000;24:488–91.
9. Allaire PE, Wood HG, Awad RS, Olsen DB. Blood flow in a continuous flow ventricular assist device. *Artif Organs* 1999; 23:769–73.
10. Burgreen GW, Antaki JF, Wu ZJ, Holmes AJ. Computational fluid dynamics as a development tool for rotary blood pump. *Artif Organs* 2001;25:336–40.
11. Nosé Y. A rotary blood pump: its design and development strategy. *Artif Organs* 1997;21:263–4.
12. Kawahito K, Nosé Y. Hemolysis in different centrifugal pumps. *Artif Organs* 1997;21:323–6.
13. Takami Y, Makinouchi K, Nakazawa T, et al. Hemolytic characteristic of a pivot bearing supported Gyro centrifugal pump (C1E3) simulating various clinical applications. *Artif Organs* 1996;20:1042–9.
14. James NL, Wilkinson CM, Lingard NL, van der Meer AL, Woodard JC. Evaluation of hemolysis in the ventrassist implantable rotary blood pump. *Artif Organs* 2003;27:108–13.
15. Yamane T, Asztalos B, Nishida M, et al. Flow visualization as a complementary tool to hemolysis testing in the development of centrifugal blood pump. *Artif Organs* 1998;22:375–80.
16. Blackshear PL, Blackshear GL. Mechanical hemolysis. In: Skalak R, Chien S, eds. *Handbook of Bioengineering*. New York: McGraw-Hill, 1987;15.1–15.19.
17. Williams AR. Shear-induced fragmentation of human erythrocytes. *Biorheology* 1973;10:303–11.
18. Champion JV, North PF, Coakley WT, Williams AR. Shear fragility of human erythrocytes. *Biorheology* 1971;8:23–9.
19. Leverett LB, Hellums JD, Alfrey CP, Lynch EC. Red blood cell damage by shear stress. *Biophys J* 1972;12:257–73.
20. Sutera SP, Mehrjardi MH. Deformation and fragmentation of human red blood cells in turbulent shear flow. *Biophys J* 1975;15:1–11.
21. Croce PA. *Hemolysis of Erythrocytes in Laminar and Turbulent Shear Flows*. PhD Thesis. Department of Mechanical and Aerospace Engineering, Washington University in St. Louis, 1972.
22. Hellums JD, Brown CH. Blood damage by mechanical forces. In: Hwang NHC, Normann NA, eds. *Cardiovascular Flow Dynamics and Measurements*. Baltimore, MD: University Park Press, 1977;799–823.
23. Hashimoto S. Erythrocyte destruction under periodically fluctuating shear rate: comparative study with constant shear rate. *Artif Organs* 1989;13:458–63.
24. Heuser G, Opitz R. A Couette viscometer for short time shearing of blood. *Biorheology* 1980;17:17–24.
25. Wurzinger LJ, Opitz R, Eckstein H. Mechanical blood trauma. An overview. *Angeiologie* 1986;38:81–97.
26. Giersiepen M, Wurzinger LJ, Opitz R, Reul H. Estimation of shear stress-related blood damage in heart valve prostheses—in vitro comparison of 25 aortic valve. *Artif Organs* 1990;13: 300–6.
27. Bludszuweit C. Three-dimensional numerical prediction of stress loading of blood particles in a centrifugal pump. *Artif Organs* 1995;19:590–6.
28. Yeleswarapu KK, Antaki JF, Kameneva MV, Rajagopal KR. A mathematical model for shear-induced hemolysis. *Artif Organs* 1995;19:576–82.
29. Yeleswarapu KK, Kameneva MV, Rajagopal KR, Antaki JF. The flow of blood in tubes: theory and experiments. *Mechanics Res Commun* 1998;25:257–62.
30. Hénon S, Lenormand G, Richert A, Gallet F. A new determination of the shear modulus of the human erythrocyte membrane using optical tweezers. *Biophys J* 1999;76:1145–51.
31. Schmid-Schönbein H, Wells R. Fluid drop-like transition of erythrocytes under shear. *Science* 1969;165:288–91.
32. Hochmuth RM. Properties of red blood cells. In: Skalak R, Chien S, eds. *Handbook of Bioengineering*. New York: McGraw-Hill, 1987;12.1–12.17.
33. Fischer TM, Stöhr-Liesen M, Schmid-Schönbein H. The red cell as a fluid droplet: tank tread-like motion of the human erythrocyte membrane in shear flow. *Science* 1978;202:894–6.
34. Pinotti M, Rosa ES. Computational prediction of hemolysis in a centrifugal ventricular assist device. *Artif Organs* 1995;19: 267–73.
35. Mitoh A, Yano T, Sekine K, et al. Computational fluid dynamics analysis of an intra-cardiac axial flow pump. *Artif Organs* 2003;27:34–40.
36. Chan WK, Wong YW, Ding Y, Chua LP, Yu SCM. Numerical investigation of the effect of blade geometry on blood trauma in a centrifugal blood pump. *Artif Organs* 2002;26:785–93.
37. De Wachter D, Verdonck P. Numerical calculation of hemolysis levels in peripheral hemodialysis cannulas. *Artif Organs* 2002;26:576–82.
38. *F1841-97 Designation: Standard Practice for Assessment of Hemolysis in Continous Flow Blood Pumps.* West Conshohocken, PA: ASTM International, 1997;1326–30.
39. Barthès-Biesel D, Rallison JM. The time-dependent deformation of a capsule freely suspended in a linear shear flow. *J Fluid Mechanics* 1981;113:251–67.
40. Maffettone PL, Minale M. Equation of change for ellipsoidal drops in viscous flow. *J Non-Newtonian Fluid Mechanics* 1998;78:227–41.
41. Roscoe R. On rheology of a suspension of viscoelastic spheres in a viscous liquid. *J Fluid Mechanics* 1967;29:273–93.
42. Keller SR, Skalak R. Motion of a tank-treading ellipsoidal particle in a shear flow. *J Fluid Mechanics* 1982;120:27–47.
43. Nonaka K, Linneweber J, Ichikawa S, et al. Development of the Baylor Gyro permanently implantable centrifugal blood pump as a biventricular assist device. *Artif Organs* 2001;25: 675–82.
44. Nosé Y. Design and development strategy for the rotary blood pump. *Artif Organs* 1998;22:438–46.

APPENDIX A

A deformed droplet returns to its natural configuration according to,

$$\frac{d\mathbf{S}}{dt} = -f_1(\mathbf{S} - g(\mathbf{S})\mathbf{I}). \qquad \text{(A-1)}$$

For small deformations $\mathbf{S} = \mathbf{I} + \varepsilon\mathbf{A}$. The eigenvalues λ_i of $\mathbf{S}$ are:

$$\lambda_i = 1 + \varepsilon\mu_i, \qquad \text{(A-2)}$$

where μ_i are the eigenvalues of **A**. Substituting $\mathbf{S} = \mathbf{I} + \varepsilon\mathbf{A}$ in Eq. A-1 yields:

$$\varepsilon \frac{d\mathbf{A}}{dt} = -f_1(\mathbf{I} + \varepsilon\mathbf{A} - g(\mathbf{S})\mathbf{I}), \quad \text{(A-3)}$$

where $g(\mathbf{S}) = 3III/II$. Consequently, the second and the third invariants of **S** become:

$$II = 3 + 2\varepsilon(\mu_1 + \mu_2 + \mu_3) + O(\varepsilon^2), \quad \text{(A-4)}$$

$$III = 1 + \varepsilon(\mu_1 + \mu_2 + \mu_3) + O(\varepsilon^2), \quad \text{(A-5)}$$

but the volume of droplet is preserved ($dIII/dt = 0$), thus $\mathrm{tr}(\mathbf{A}) = \mu_1 + \mu_2 + \mu_3 = 0$. Neglecting the $O(\varepsilon^2)$ terms leads to $g(\mathbf{S}) = 1$. Substituting $g(\mathbf{S})$ in Eq. A-3 we get:

$$\frac{d\mathbf{A}}{dt} = -f_1\mathbf{A}. \quad \text{(A-6)}$$

The solution to this equation is of the form:

$$\mathbf{A} = \mathbf{A}_0 \exp(-f_1 t), \quad \text{(A-7)}$$

where $1/f_1$ is the relaxation time. Because the relaxation time of RBC membrane is 200 ms we set $f_1 = 5\ \mathrm{s}^{-1}$.